Identification of Stable Species Formed Under CO Adsorption and Oxidation on Alumina-Supported Single Pt Atoms: Why Nanoparticles Are More Active

F. Morfin, Caroline Dessal, Alexis Sangnier, Céline Chizallet, L. Piccolo

Identification of Stable Species Formed under CO Adsorption and Oxidation on Alumina-supported Single Pt Atoms: Why Nanoparticles are More Active

Franck Morfin,[1] Caroline Dessal,[1] Alexis Sangnier,[2] Céline Chizallet,[2,*] Laurent Piccolo[1,*]

[1] *IRCELYON, CNRS & Université Lyon 1, 69100 Villeurbanne, France*

[2] *IFP Energies nouvelles, Rond-point de l'échangeur de Solaize, BP3, 69360 Solaize, France*

* Corresponding authors: Laurent.Piccolo@ircelyon.univ-lyon1.fr; Celine.Chizallet@ifpen.fr

Abstract

Single-atom catalysis is attractive in the context of sustainable chemistry, but single-atom catalysts (SACs) are not always more active than corresponding clusters or nanoparticles. This is the case, *inter alia*, of CO oxidation on Pt/γ-Al_2O_3, an archetypal catalytic system where SACs are poorly active. In the present work combining diffuse reflectance infrared spectroscopy experiments and density functional theory calculations, we identity the stable species formed on a Pt/γ-Al_2O_3 SAC compared to its nanocatalyst counterpart. Formates predominantly occupy the alumina support sites, while oxidized Pt_1 species can stabilize carbonyl, carbonate and bicarbonate species, depending on the temperature regime. Co-adsorption of carbonyl and carbonate moieties on the same platinum atom is found likely from both experimental and thermodynamic arguments. Unlike the mild adsorption of CO on Pt clusters allowing for efficient CO oxidation, carbonyl and carbonate species exhibit high stability on the single Pt atoms, which can explain the low activity of the SAC.

Keywords

Single-atom catalysis, CO oxidation, Pt/Al_2O_3, DRIFTS, density functional theory, carbonates

1. Introduction

After a decade of considerable expansion, single-atom catalysis has become a major field of heterogeneous catalysis, especially because supported single atoms can exhibit novel catalytic properties with respect to conventional nanocatalysts (NCs).[1–6] Pioneering studies in this field have considered noble metal atoms (Rh, Pd, Pt, Au) supported on transition metal oxides (alumina, magnesia, ceria, iron oxide) for oxidation reactions.[7–15] The transposition of mechanisms known for NCs to single-atom catalysts (SACs) is not always obvious, due to the lack of multiple metallic adsorption sites. Moreover, depending on the reaction under consideration, it remains unclear whether single atoms (SAs) are more or less active than clusters or nanoparticles (NPs). This question is particularly debated in the case of the emblematic CO oxidation reaction.

In 2013, Moses-DeBusk *et al.* reported an investigation of CO oxidation over atomically dispersed 0.18 wt% Pt/θ-Al_2O_3 and proposed a reaction pathway involving preferential oxygen adsorption and Pt carbonate formation without any contribution of the support, except for the stabilization of the single atom itself.[16] In contrast, Ding *et al.* found that CO strongly adsorbs on oxide-supported Pt SAs, which inhibits their catalytic activity in both CO oxidation and water-gas shift at low temperatures.[17] Using a commercial Pt/Al_2O_3 catalyst and transient experiments, Newton *et al.* proposed a cooperative CO oxidation mechanism involving both Pt NPs and SAs.[18,19] The former would store CO and dissociate O_2, while oxidized Pt SAs would react with CO to form bidentate carbonates serving as reaction-intermediate species. Without the presence of NPs, the SAs are considered inactive. Using an ultralow Pt loading of 0.044 wt%, Lou and Liu measured a turnover frequency (TOF) of 0.9×10^{-2} s^{-1} at 160 °C for Pt_1/γ-Al_2O_3, whereas it is 16.5×10^{-2} and 33.2×10^{-2} for ZnO and Fe_2O_3-supported counterparts, respectively.[20] This result suggests that alumina-supported Pt SAs possess a low but non-zero intrinsic CO oxidation activity (in agreement with Moses-DeBusk *et al.*), which can be boosted by the presence of a reducible oxide support. The CO oxidation activity of Pt SAs was also reported by Zhang *et al.* for 0.2 wt% Pt/m-Al_2O_3 (mesoporous) catalysts[21] and by Wang *et al.* for 0.4 wt% Pt/La-Al_2O_3 catalysts stabilized with barium.[22]

Some of us previously investigated CO oxidation over atomically dispersed 0.3 wt% Pt/γ-Al_2O_3 by means of *operando* infrared and X-ray absorption spectroscopies. We found that cationic Pt SAs are poisoned with strongly bound CO (in agreement with Ding *et al.*) and easily diffuse on the alumina surface, leading to the gradual formation of active nanometer-sized clusters; the aggregation process is enhanced at higher Pt loading or lower O_2/CO ratio.[23] Thus, it became clear that alumina-supported Pt clusters are much more active than SAs. However, an intrinsic activity of the SAs and a possible role of carbonate species could not be excluded, that may be hidden by the effects of the clustering process.

Herein, we employ *operando* diffuse reflectance infrared spectroscopy (DRIFTS) experiments and density functional theory (DFT) calculations to determine the nature of stable carbon-containing species on γ-alumina-supported Pt SAs as compared to clusters in CO oxidation conditions. Stable carbonyls are observed on oxidized forms of Pt SAs, as well as carbonates and bicarbonates depending on the temperature regime. We show that carbonyl and carbonate moieties can co-adsorb on Pt SAs, and that the high adsorption energies of these species are likely at the origin of activity inhibition.

2. Materials and Methods

2.1. Catalyst preparation

γ-Al_2O_3 powders (Sasol Puralox SCFa-140) were calcined in air at 600 °C for 3 h before use. The catalysts were prepared by incipient wetness impregnation: 2.0 g of alumina were impregnated with 1.8 mL of an aqueous solution of $Pt(NH_3)_4(NO_3)_2$ (Alfa Aesar, >50 wt% Pt), dried in air at 60 °C for 5 h, and calcined in air (40 mL/min) at 300 °C for 2 h (2 °C/min ramp). The Pt loadings of the 0.3Pt and 1Pt samples were find equal to 0.31 wt% and 0.96 wt%, respectively, by inductively coupled plasma - optical emission spectroscopy (ICP-OES, Horiba Jobin Yvon).

2.2. Materials characterization

The STEM-HAADF experiments were performed with a FEI Titan ETEM G2 electron microscope equipped with a Cs image aberration corrector and operated at 300 keV. The extraction voltage, camera length, acceptance angles, STEM resolution and probe current were 4500 V, 245 mm, 29.2-146 °, 0.14 nm and <0.1 nA, respectively. For sample preparation, the powder was crushed and dispersed in ethanol through ultrasonication, dropped onto a holey carbon-coated 200 mesh Cu grid, and dried by a lamp. To avoid contamination during analysis and remove all residual carbon, the samples were Ar plasma-cleaned for 20 s (Plasma Prep 5, GaLa Instrumente). No filtering was applied on the STEM images.

2.3. *Operando* DRIFTS

Operando infrared spectroscopy experiments were performed with a Thermo Nicolet 6700 FTIR spectrophotometer equipped with a DRIFTS cell (Harrick HVC-DRP) and a high-sensitivity MCT detector. The cell, equipped with CaF_2 windows, was connected to a gas handling system allowing for *in situ* treatments with several gases at temperatures up to 500 °C. About 30 mg of the powder sample was placed in the cell sample holder. The sample was submitted to the following treatments or reactions at atmospheric pressure with a total flow rate of 25 mL/min: (i) 20% O_2 in He, 2 °C/min, 350 °C, 2 h; (ii) 2% CO + 2 or 10% O_2 in He, 2 cycles; (iii) H_2, 2 °C/min, 350 °C, 2 h; (iv) identical to (ii); (v) identical to (i); (vi) identical to (ii). Figure S1 allows visualizing this protocol. The spectra were recorded in the 1000–4000 cm^{-1} range at a resolution of 2 cm^{-1} by accumulating 64 scans. The Omnic software (Thermo) was used for initial data processing. Temperature cycles were composed of ramps (3 °C/min) and plateaus (20 min, for DRIFTS acquisition) every 50 °C. The reported temperature corresponds to that of the powder sample surface after calibration with a pyrometer. The gases exiting the DRIFTS cell were continuously monitored with a mass spectrometer (Aspec QMS from SRA Instruments). The experiments were also performed with bare γ-Al_2O_3, and they were used to subtract the signal of gaseous CO from the DRIFTS spectra by considering that CO adsorption on bare alumina is negligible at the temperatures considered. The recorded spectra were smoothed via the Savitzky-Golay algorithm (50 pts

windows and second-order polynomial) and a baseline was subtracted (asymmetric least squares algorithm) with Origin software.

2.4. Density functional theory calculations

Periodic DFT calculations were performed with the VASP code [24,25] with the PBE (Perdew, Burke, and Ernzerhof) exchange–correlation functional,[26] using the projected augmented wave (PAW) method [27] to describe the core-electrons interactions. The plane wave basis set was limited to a kinetic cut-off energy of 400 eV. The convergence criterion for the electronic self-consistent field relaxation was fixed to 10^{-6} eV, and all calculations were performed at the Γ-point. The models consist in platinum single atoms dispersed over the dehydrated (100) γ-Al_2O_3 surface. The support model comes from the work of Digne *et al.*,[28,29] used with a 2×3 multiplicity, later modified by the adsorption of platinum atoms[30] and clusters.[31] This surface, which is dehydrated and dehydroxylated in a large range of operating conditions typical of the present work,[29,32,33] provides strong anchoring sites for Pt SAs, stronger than hydrated (110) facets.[30] The (100) facet was used in a series of previous works to describe the support interaction with Pt clusters[31,34–37] and SAs,[38,39] and was shown to be a reasonable choice regarding the comparison with experimental features. CO adsorption was modeled for various supported PtO_x species found in ref.[38]. Geometries of CO-covered supported Pt_{13} clusters $Pt_{13}(CO)_9$ and $Pt_{13}(CO)_{12}$ are taken form ref.[36] Additional cluster structures are computed, associating oxygen and CO-derived adsorbates (carbonyls, formates, bicarbonates, carboxyls, and carbonates), starting from supported $Pt_{13}O_x$ models proposed in ref. [35].

Geometry optimizations were made with a convergence criterion on forces of 0.02 eV.$Å^{-1}$, by relaxing two alumina layers, the single atom and its adsorbates. Harmonic vibration frequencies were computed by the finite difference method, with a displacement of ±0.01 Å in each direction for all relaxed atoms. Similar as in ref. [36], for the CO elongation modes of adsorbed CO molecules, the reported frequencies are the computed ones blue-shifted by 21 cm^{-1}, as isolated CO is computed to vibrate at 2122 cm^{-1}, whereas it is known experimentally to be at 2143 cm^{-1}. All other frequencies (corresponding to

carbonates, bicarbonates, carboxyls, and formates) are reported as computed. On a selection of systems, the density functional perturbation theory (DFPT) was used to compute intensities of the various vibration modes. Free energies were computed from the vibration frequencies obtained by the finite difference method, assuming a complete loss of the translation and rotation modes of the molecules once adsorbed.

3. Results

3.1. DRIFTS experiments

Based on STEM, *operando* XAS, and *operando* DRIFTS, our previous works have led to the following conclusions:[23,38] i- As-prepared pre-calcined samples are atomically dispersed. At a Pt loading up to 0.3 wt%, the catalyst is single atomic, while at higher loading (typically 1 wt%) the catalyst also contains a fraction of subnanometric oxidic clusters. ii- Upon thermal treatment in H_2 or in the course of the heating/cooling CO oxidation cycles, atomically dispersed cationic Pt species aggregate into nanometric Pt clusters with superior CO oxidation activities. An increase in the Pt loading or the CO/O_2 concentration ratio accelerates the clustering-reduction phenomenon.

Herein, the SAC refers to an as-prepared 0.3 wt% Pt/γ-Al_2O_3 catalyst (0.3Pt sample), while the NC is a 1 wt% Pt/γ-Al_2O_3 catalyst (1Pt sample) having previously encountered reducing conditions. Figure 1 shows typical STEM images of the two samples. Figure S2 reports the corresponding catalytic data obtained with a conventional flow fixed-bed reactor.[23] For $CO:O_2$=2:10% at 150 °C (CO conversion lower than 6%), the activities of the SAC and the NC are 13 and 64 $mol_{CO}\ mol_{Pt}\ s^{-1}$ (0.21 and 3.2 $mmol_{CO}\ g_{cat}^{-1}\ h^{-1}$), respectively.

DRIFTS experiments were performed in three different conditions: CO oxidation with $CO:O_2$=2:10% (COOX10), CO oxidation with $CO:O_2$=2:2% (COOX2), and CO desorption. Bare alumina, 0.3Pt and 1Pt samples were investigated. For each condition and loading, the experiments included a series of heating/cooling cycles with the following steps: air calcination treatment, CO oxidation (2 cycles) or desorption, H_2 reduction treatment, CO oxidation (2 cycles) or desorption, air calcination treatment, CO

oxidation (2 cycles) or desorption, as illustrated in Figure S1. For both samples, the CO oxidation or desorption DRIFTS sequence was preceded by an oxidative calcination step, in order to avoid artifacts related to different pretreatments. The whole set of COOX DRIFTS data is reported in SI, Figures S3-S7. Note that for reaction experiments, pre-reduced 0.3Pt and pre-oxidized 1Pt also present some features relevant to the NC and the SAC, respectively. Moreover, the second cycle after pretreatment generally retains similar features as in the first cycle (the main exceptions are discussed below).

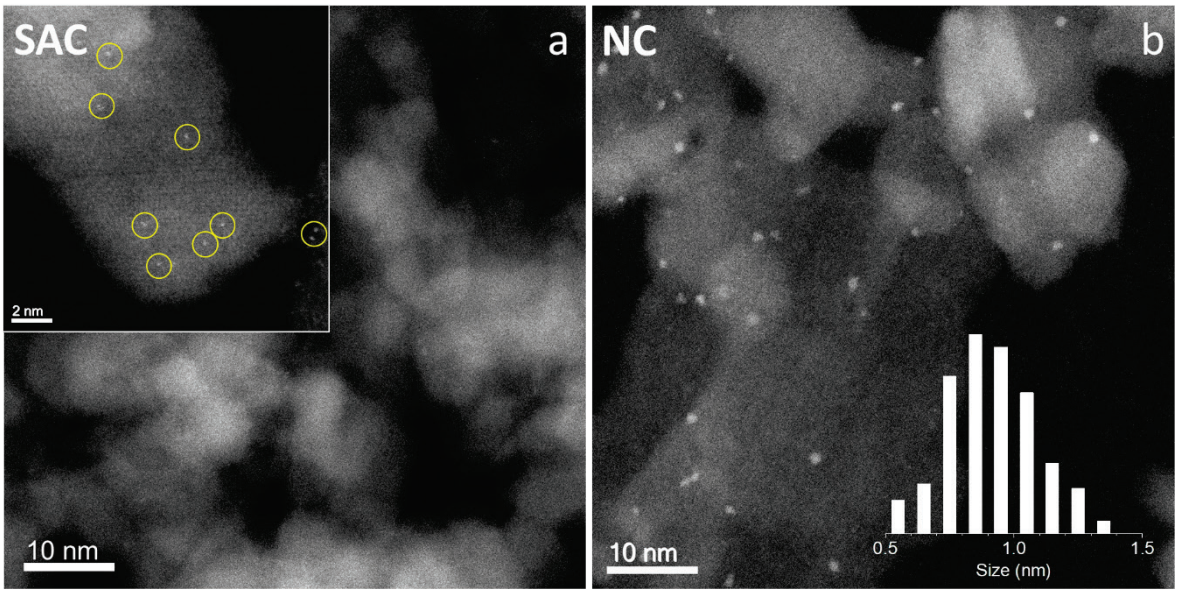

Figure 1. STEM-ADF images of a) 0.3 wt% Pt/γ-Al_2O_3 calcined at 300 °C in air (single-atom catalyst, SAC, the circles in the insert locate single Pt atoms) and b) 1.0 wt% Pt/γ-Al_2O_3 reduced at 300 °C in H_2 (nanocatalyst, NC).

Figure 2 gathers the data for the SAC, the NC, and bare alumina under heating/cooling COOX10 conditions, in the form of color maps in the 2400-1200 cm^{-1} wavenumber range. Figure 3 allows a more quantitative comparison between the main IR band intensities for the SAC and the NC. Finally, Figures S8 and S9 report the DRIFTS data for CO desorption experiments. The IR bands have been ascribed (Table 1) on the basis of the existing literature, including our previous work.[23,40–43] Notably, these

assignments are qualitatively confirmed by our DFT calculations, although the splitting between the two detected modes of carbonates is usually overestimated by DFT, as will be discussed in **Section 3.2**. The identification of formate species also required the simultaneous analysis of high-frequency vibrations near 3000 cm^{-1} corresponding to C-H stretching, as shown in Figure S10. Formates are mostly visible on bare alumina, though small contributions can be detected on 0.3 wt% Pt/Al_2O_3, whether after calcination (SA state) or reduction (mostly cluster state). They are absent from the 1 wt% Pt/Al_2O_3 catalyst. This may indicate that either Pt SAs somewhat stabilize the formates, or Pt covers their adsorption sites at high loading.

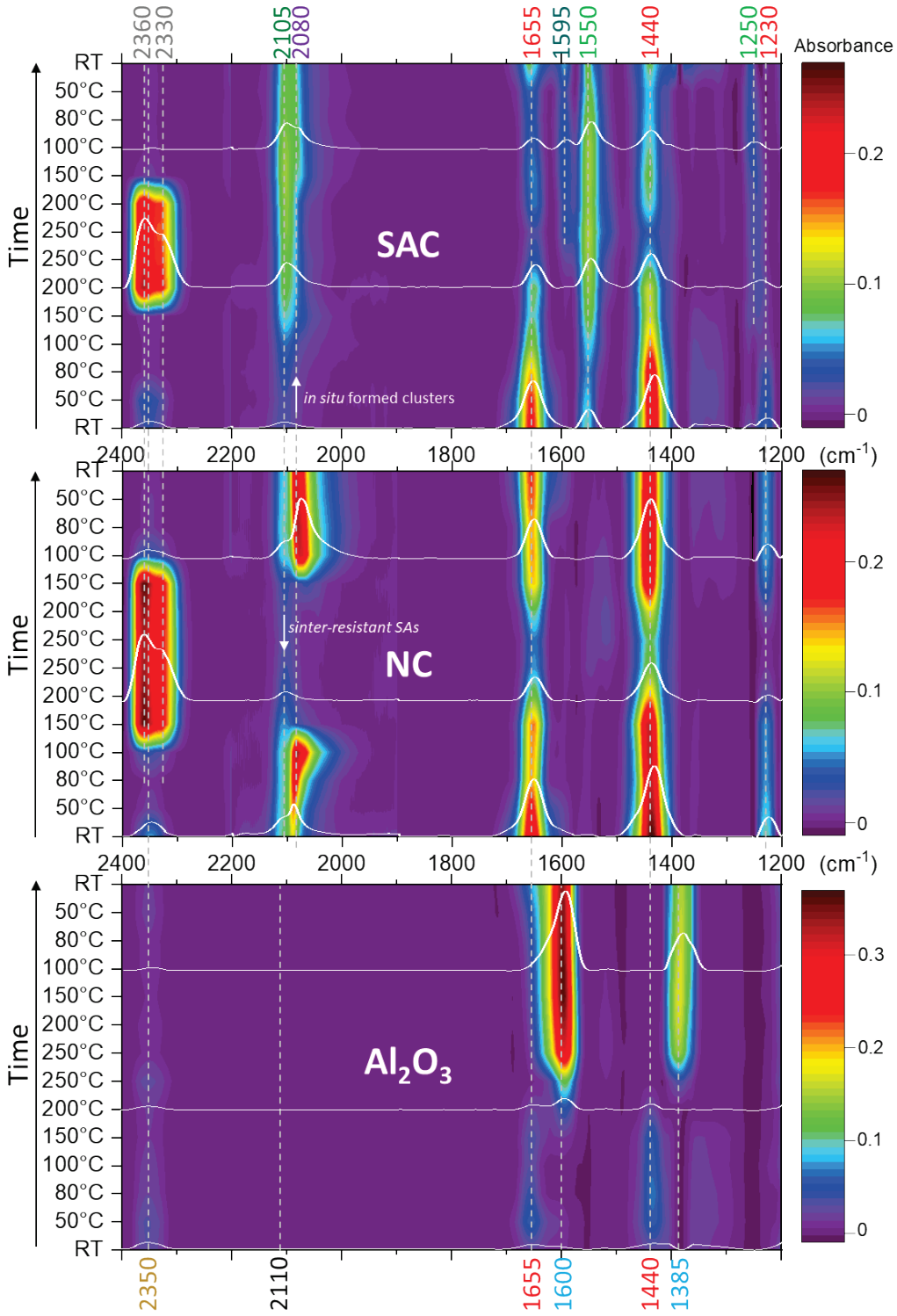

Figure 2. CO oxidation DRIFTS experiments, under COOX10 conditions, for the single-atom catalyst (top), the nanocatalyst (middle), and the bare alumina support (bottom). The C-O stretching vibration signal measured for alumina was subtracted from all the spectra.

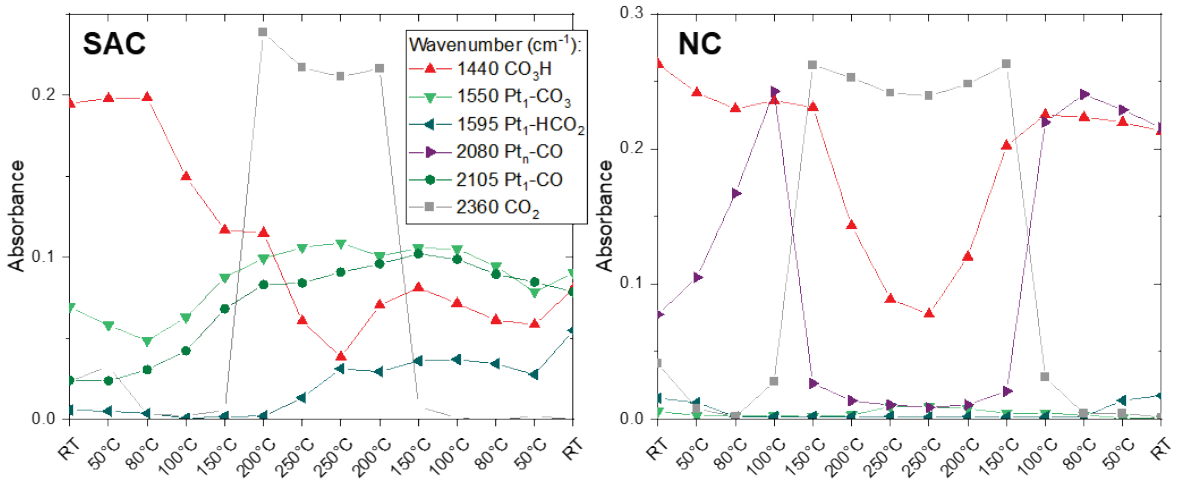

Figure 3. Evolution of the intensities of the main DRIFTS bands during CO oxidation experiments on Pt/Al_2O_3 catalysts (time runs from left to right).

Table 1. Assignment of the main observed IR absorption bands. S, N and A refer to the single-atom catalyst, the nanocatalyst and the alumina support, respectively.

σ (cm^{-1})	Material	Assignment	Vibration mode
1230	S N	Bicarbonate	δCOH
1250	S	Carbonate	ν_{as}COO
1385	A	Formate	ν_{sy}COO
1440	S N A	Bicarbonate	ν_{sy}COO
1550	S	Carbonate	νC=O
1595	S	Formate	ν_{as}COO
1600	A	Formate	ν_{as}COO
1655	S N A	Bicarbonate	ν_{as}COO
2080	N (S)	Linear carbonyl	νCO
2105	S (N)	Linear carbonyl	νCO
2330	S N	Gaseous linear CO_2	ν_{as}COO
2350	S N A	Physisorbed linear CO_2	ν_{as}COO
2360	S N	Gaseous linear CO_2	ν_{as}COO

Figures 2 and 3 and Table 1 reveal a quite different behavior between the SAC and the NC. As previously reported by some of us,[23] the temperature window of CO_2 production (band around 2350 cm^{-1}) is wider

for the NC, and correlates with the extinction of the Pt-CO band – centered at *ca.* 2080 cm^{-1} – owing to low CO coverage at high conversion. Note that the CO oxidation process combined to our thermal ramping procedure leads to only two observable regimes in DRIFTS-MS: no activity before light-off, and 100% conversion upon light-off.[23] For the SAC, the main Pt carbonyl band is centered at *ca.* 2105 cm^{-1} and corresponds to single Pt cations (which will be confirmed later in the section devoted to the DFT results); this band shows a shoulder at 2080 cm^{-1} during the cooling phase, which is ascribed to *in situ* formed Pt clusters with slightly positive oxidation degree.[23] As expected, the shoulder contribution is weak at high temperature due to CO conversion on the clusters. In contrast, the main band at 2105 cm^{-1} is roughly constant, which made us rule out any CO oxidation activity of the SAs. The initial increase in the band intensity was ascribed to the initial saturation of Pt SAs with oxygen adsorbates.[16,23] This band is also present on the NC as a small peak or shoulder to the 2080 cm^{-1} band, and is ascribed to sinter-resistant SAs.

Now, let us analyze the features at lower wavenumbers (<1700 cm^{-1}). From Figure 2, common features between the SAC and the NC at low temperature are bands at 1655, 1440, and 1230 cm^{-1}, which relate to bicarbonate (CO_3H) species (Table 1). However, their thermal evolution is different between the two catalysts both in decreasing behavior on heating and in reversibility on cooling, the bicarbonate partial disappearance being reversible only on the NC: bicarbonates can (reversibly) decompose into carbonates or desorb in the form of CO_2. Bicarbonate species are also present on alumina at low temperature (Figure 2), though in lower amount than on the Pt catalysts. Moreover, they disappear above 200 °C and partially reappear on cooling. As expected from the previous decomposition of bicarbonates, during the second cycle of reaction on the pre-oxidized samples, the bicarbonate bands (1655 and 1440 cm^{-1}) are less intense on heating with respect to the first cycle (Figures S3-S5, C300-A2). The CO desorption data of Figure S8 further show that bicarbonates are also present on the catalysts in the absence of O_2.

In addition, bands at 1250 and 1550 cm^{-1} are exhibited by the SAC only. They could be ascribed to a chelating bidentate Pt carbonate (Pt_1-CO_3) species (Table 1).[40] The thermal evolution of the 1550 cm^{-1} band (Figure 3) is not correlated to CO_2 production, but instead exhibits a similar trend as the Pt_1-CO

band at 2105 cm^{-1}. This species is present only on pre-calcined samples, both under COOX10 and COOX2 conditions (Figures S3-S5). Its absence after a reduction or an additional calcination supports its assignment to a SAC-specific species. Since COOX2 conditions are more reducing, they lead to faster sintering of SAs compared to COOX10 conditions.[23] Apart from this fact and the promotion of the formate species, the data recorded under both conditions present similar patterns.

For the SAC, the respective evolutions of bicarbonate and Pt carbonate bands from 80 °C to 200 °C suggest a possible decomposition of the bicarbonate to the Pt carbonate, while the latter is already present at room temperature (RT). In any case, the carbonate species is stable and coexists with the Pt carbonyl. The hypothesis of bicarbonate conversion to Pt carbonate on the SAC is supported by the CO desorption experiments (Figures S8 and S9). In this case, the carbonyl species is much less abundant than under COOX conditions, which supports the fact that CO is not a product of bicarbonate decomposition. The initial presence of O ligands around the single Pt atoms[38] may favor the formation of bicarbonates at the expense of carbonyls, CO being absent from the gas flow during the desorption experiments.

Finally, another feature is visible above 200 °C, only for the 0.3Pt SAC under COOX10 conditions: the small band centered at 1595 cm^{-1} may be ascribed to a Pt formate. It is known that formates are produced at relatively high temperatures upon interaction of CO with OH groups.[40] This species reinforces during the next COOX cycle, and is also detected on the 0.3Pt catalyst after reduction, both in COOX10 (Figure S4) and COOX2 (Figure S5) conditions. Moreover, it is visible in the CO desorption experiments on the SAC, including at low temperature (Figure S10). However, the fact that this species is also present after the reduction step suggests that it is not SAC-specific.

It can be noticed that hydroxyl groups are necessarily present on alumina surfaces. Figure S11 reports the features detected in the high-frequency region during a $CO+O_2$ temperature cycle on alumina. They are representative of the signal detected for all the samples and typical of OH groups on γ-alumina (their

assignment has been discussed in previous studies).[29,44–47] Their amount is seen to decrease upon heating to 300 °C, and increase back upon cooling to RT.

3.2. DFT calculations

DFT calculations were performed to further evaluate the stability of molecular adsorbates, starting from alumina-supported Pt_1, Pt_1O_2, or Pt_1O_4 models, and gradually adding CO molecules, leading to Pt carbonyl and carbonate species. The Pt_1O_4 stoichiometry is consistent with the results of extended X-ray absorption fine structure spectroscopy (EXAFS) on pre-calcined Pt/Al_2O_3 SACs, while Pt_1O_2 is more favorable in the presence of CO.[23,38] Hydration was also simulated to model bicarbonate, carboxyl, and formate species, with a participation of the support to host the complementary hydroxyl/proton species. Figure 4 shows the most stable molecule/catalyst models together with the energy gain at each step, while Table 2 reports the computed vibration wavenumbers of the corresponding adsorbed species. Figure S12 provides a synopsis of the distribution of computed frequencies grouped by family of vibrator. Note that while the number of Al atoms from the support coordinated to ligands of the Pt atoms is mentioned in Table 2, this data is not mentioned in the following text for the sake of clarity.

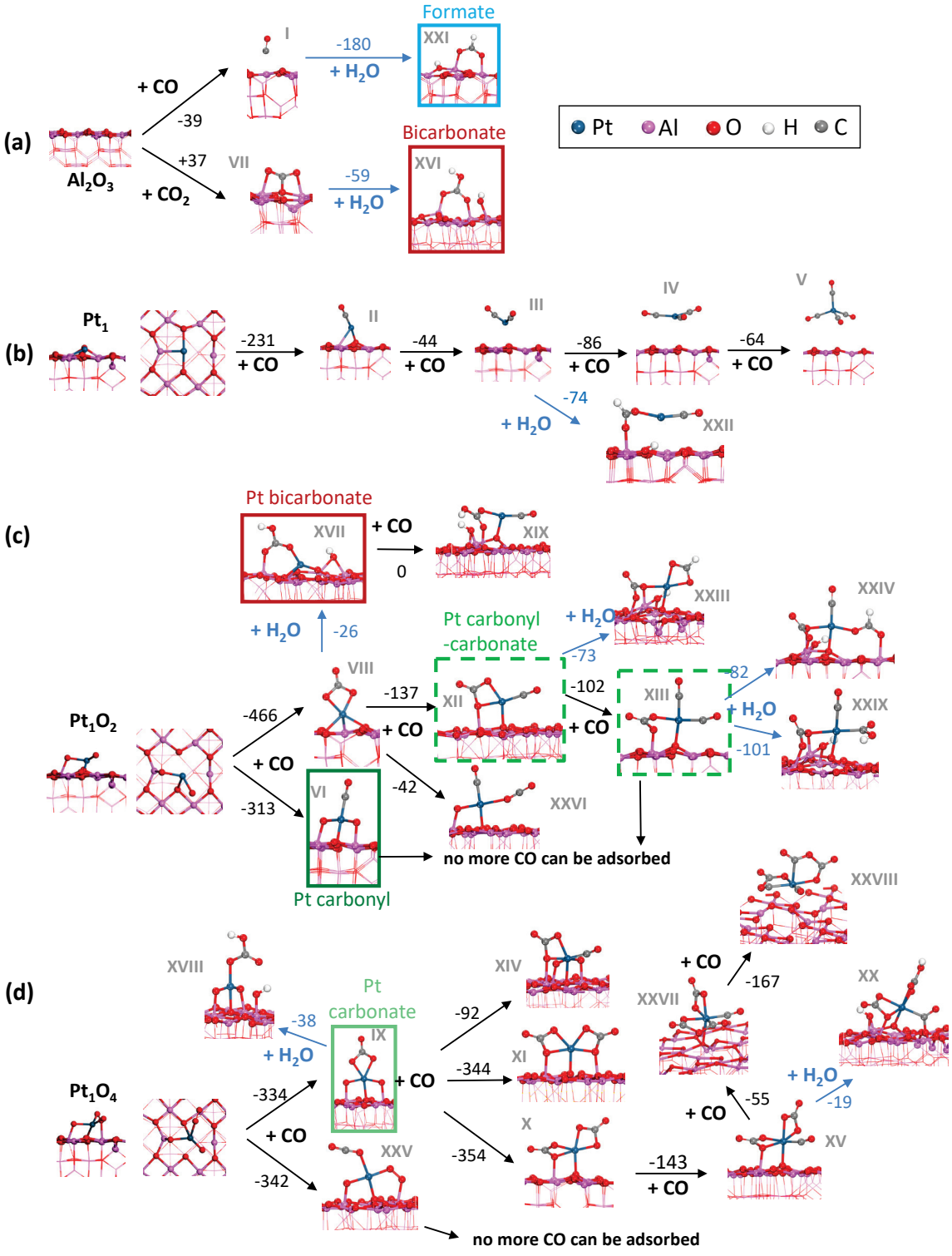

Figure 4. DFT optimized models of CO adsorption and hydration on alumina (a) and on single Pt atom supported on alumina either in the Pt_1 (b), Pt_1O_2 (c), or Pt_1O_4 (d) form. The number values represent CO, CO_2 or H_2O adsorption energies in kJ/mol. Frames shed light on the most probable species, from comparison with DRIFTS experiments (plain lines) and from stability arguments (doted lines).

*Table 2. DFT-computed vibration wavenumbers (cm^{-1}) for selected Pt single atom species adsorbed on alumina. Numbers in italic correspond to shifted wavenumbers (see **Section 2.4**). When computed, the intensity of the mode is reported between brackets in arbitrary units. The underlined Roman numerals correspond to the most probable species.*

Carbonyl		
I	Al(CO)	*2172 (0.2)*
II	Pt(CO)	*2058 (0.8)*
III	$Pt(CO)_2$	*2073 (0.9), 2014 (1.6)*
IV	$Pt(CO)_3$	*2090 (0.5), 2035 (1.2), 2027 (1.3)*
V	$Pt(CO)_4$	*2101 (0.1), 2047 (0.3), 2042 (0.6), 2038 (1.0)*
VI	$Pt(O)_2(CO)Al_2$	*2119 (0.9)*
Carbonate and carbonyl-carbonate		
VII	$Al_2(CO_3)$	1737, 1268, 888, 855
VIII	$Pt(CO_3)$	1780, 1077
IX	$Pt(O)_2Al_2(CO_3)$	1691 (0.2), 1228 (0.1)
X	$Pt(CO_3)_2Al$	1814, 1741, 1185, 1097
XI	$Pt(CO_3)_2Al_2$	1795, 1786, 1129, 1111
XII	$Pt(CO)(CO_3)Al$	*2094 (0.8)*, 1806 (0.7), 1097 (0.6)
XIII	$Pt(CO)_2(CO_3)Al$	*2145 (1.3), 2084 (0.7)*, 1720 (0.5), 1134 (0.4)
XIV	$Pt(O)_2Al_3(CO)(CO_3)$	*2149*, 1771, 1081
XV	$Pt(CO)(CO_3)_2Al$	*2147*, 1808, 1752, 1137, 1092
Bicarbonate, carbonate-bicarbonate, and carbonyl-carbonate-bicarbonate		
XVI	$Al_2(CO_3H)$	3675 (0.1), 1635 (0.6), 1443 (0.6), 1200 (0.5), 1059 (0.2)
XVII	$Pt(CO_3H)Al$	3669 (0.1), 1610 (0.5), 1435 (0.5), 1188 (0.8), 1045 (0.1)
XVIII	$Pt(O)_2Al_2(CO_3H)$	3672, 1714, 1249, 1135, 940
XIX	$Pt(CO)(CO_3H)Al$	3658, *2080*, 1595, 1426, 1186, 1053
XX	$Pt(CO)(CO_3)(CO_3H)Al$	3669, 1791, 1752, 1540, 1511, 1192, 1149, 1025, 911
Formate, carbonyl-formate, carbonate-formate, and carbonyl-carbonate-formate		
XXI	$Al_2(HCO_2)$	2997(0.1), 1568 (0.7), 1378 (0.1), 1341 (0.1), 1014 (0.1)
XXII	$Pt(CO)(HCO_2)Al$	2968 (0.1), *2032 (1.0)*, 1580 (1.1), 1375 (0.1), 1351 (0.1), 1007 (1.1)
XXIII	$Pt(CO_3)Al_2(HCO_2)$	3067, 1788, 1505, 1343, 1243, 1160, 956
XXIV	$Pt(CO)(CO_3)Al_2(HCO_2)Al$	2987, *2105*, 1804, 1610, 1373, 1315, 1158, 992
Others		
XXV	$Pt(O)Al(O_2)Al(CO_2)$	2348 (0.8), 1293 (0.1)
XXVI	$Pt(O)Al(CO)(CO_2)$	2390 (0.9), *2100 (0.6)*, 1326 (0.1)
XXVII	$Pt(CO)(CO_3)(C_2O_4)Al$	*2149*, 1877, 1810, 1729, 1186, 1157, 919, 906
XXVIII	$Pt(CO)(C_2O_4)_2Al$	*2145 (0.52)*, 1896 (1.5), 1875 (1.1), 1821 (1.3), 1805 (0.4), 1261 (0.4), 1187 (0.5), 1050 (2.5), 924 (1.0)
XXIX	$Pt(CO)(CO_3)(COOH)Al_2$	3549 (0.1), *2124 (0.6)*, 1771 (0.3), 1764 (0.5), 1233 (0.5), 1159 (0.5), 1045 (0.4), 1018 (2.3)

Starting from Pt_1 (with platinum formally at zero-oxidation degree, Figure 4b), CO adsorption leads to an uplift of the single atom, similar to what hydrogen does.[38] Up to four CO molecules can be adsorbed on the Pt atom, but with more than one CO molecule the multicarbonyl desorbs from the support. Adsorbing CO on Pt_1O_2 leads to the formation of a chelating bidentate carbonate (species **VIII**), *i.e.* the same species as suggested from DRIFTS experiments. This species is more stable than the square planar O_2PtCO configuration (species **VI**), itself very similar to O/CO co-adsorption configurations computed in the case of Pt SAs anchored on TiO_2.[48] From the bidentate carbonate, further adsorption of CO leads to a $Pt(CO)(CO_3)$ species (**XII**), which itself converts into $Pt(CO)_2(CO_3)$ (**XIII**) upon additional CO chemisorption. From this dicarbonyl-carbonate or the square planar carbonyl, no more CO can be added (it was attempted, but spontaneous desorption takes place in the course of the optimization). The computation of CO adsorption free energies indicates that at 20 mbar of CO (*i.e.* like in the experiments), **XIII** is more stable than **XII** at temperatures lower than 300 °C, the stability domain of **XII** extends from 300 to 475°C, and **VIII** dominates above 475°C (Figure S13). Finally, starting from Pt_1O_4, a $Pt(O)(O_2)(CO_2)$ species (**XXV**) can be formed (adsorbed CO_2 formed spontaneously in the course of the optimization, starting from a $Pt_1O_4(CO)$ initial state). Alternatively, $Pt(O)_2(CO_3)$ (**IX**) can be formed, onto which further CO adsorption leads to stable Pt dicarbonates, $Pt(CO_3)_2$ (species **X**, **XI** or **XIV**). **X** can be converted to $Pt(CO)(CO_3)_2$ (**XV**) upon supplementary CO addition, though with lower gain in adsorption energy. Finally, two additional CO molecules can still be attached, leading to species **XXVII** and **XXVIII**. In the latter, CO-carbonate coupling occurs along the geometry optimization, with the formation of (OC)-O-(CO_2) dimers.

To account for H-containing species, a number of hydration steps were considered (Figure 4), leading to bicarbonates (species **XVI-XX**), formates (**XXI-XXIV**), and carboxyl (**XXIX**). A carbonyl and/or a carbonate group are also possibly co-adsorbed. Notably, in the $Pt(CO)(CO_3)(CO_3H)$ **XX** species, the carbonyl group bridges with an oxygen from the support to yield an interfacial CO_2 species.

As shown experimentally,[23] SAs are prone to aggregation in the presence of CO. Starting from the set of $Pt_1(CO)_n$ models ($1 \leq n \leq 4$, species **II** to **V**), and choosing as possible final states $Pt_{13}(CO)_9$ and

$Pt_{13}(CO)_{12}$ models (Figure 5a, shown to be relevant at 20 mbar CO pressure),[36] we compute a negative sintering free energy for temperatures above 80 °C (see Figure S13). This ability of CO to promote sintering of reduced Pt SAs resembles the one of H_2.[38] In the sole presence of CO, the expected transition at 80 °C is found from $Pt_1(CO)_3$ to $Pt_{13}(CO)_{12}$. Thus, for comparison, we complemented the previous set of SA models with cluster models (Figure 5). The corresponding vibration wavenumbers are reported in Table 3. In addition to the $Pt_{13}(CO)_9$ and $Pt_{13}(CO)_{12}$ models relevant to CO-rich conditions, we have selected two sets of stoichiometries, $Pt_{13}O_{22}(CO)$ (Figure 5b) and $Pt_{13}O_{16}(CO)_7$ (Figure 5c), as starting states for the genesis of adsorbed carbonates, formates, carboxyls, and bicarbonates. $Pt_{13}O_{22}$ was indeed shown to be a relevant stoichiometry in oxygen-rich atmospheres,[35] hence it is an interesting starting point to analyze the effect a single CO molecule adsorption. The resulting cluster exhibits hemispherical shape, inherited from that of $Pt_{13}O_{22}$, strongly connected to the support by Pt-O bonds. The $Pt_{13}O_{16}(CO)_7$ stoichiometry represents a case of intermediate coverage of O and CO with respect to the other cases. The morphology of this cluster is intermediate between biplanar and hemispherical shapes, in line with its behavior in pure CO [36] or O_2 [35] atmospheres. For the proposed carbonate configurations, which correspond to multidentate species with two Pt atoms and one Al atom, the formation energy is more negative for the carbonate than for the carbonyl in the case of $Pt_{13}O_{16}(CO)_7$, whereas the formation of the carbonyl is slightly more favorable in the $Pt_{13}O_{22}(CO)$ case (Figure 5). It is, however, difficult to conclude univocally about the conditions where carbonates are formed more likely at the border of clusters, as this would require a more careful investigation of the full configurational space. Among species obtained with a contribution of water, bicarbonates are more stable than carboxyls and formates, the formation of the latter being endo-energetic.

This investigation shows the importance of considering oxidized forms of Pt SAs, not solely reduced ones. A comparison can be made with results previously obtained by Thang *et al.*[48] for Pt SAs supported on anatase TiO_2: the adsorption energy of CO on reduced Pt clusters is much stronger than on PtO_2 SAs, which were found more active for CO oxidation, whereas the opposite trends are observed in the present work. Moreover, unlike for Pt/γ-Al_2O_3, in the case of Pt/TiO_2 CO was found more strongly adsorbed on

the NPs than on the SAs, which were found more active. This reveals the importance of metal-support interactions for monitoring Pt SA reactivity.

Besides, we are aware that the diversity of species in presence may be much wider than simulated here, as we have only considered the dehydrated and dehydroxylated (100) facet of γ-alumina as support for the Pt SAs and clusters. Alumina platelets indeed exhibit much more diverse sites, due to other facets[29,33] and edges[49,50] – some of these being hydroxylated – for which surface models are available, opening perspectives to the current work.

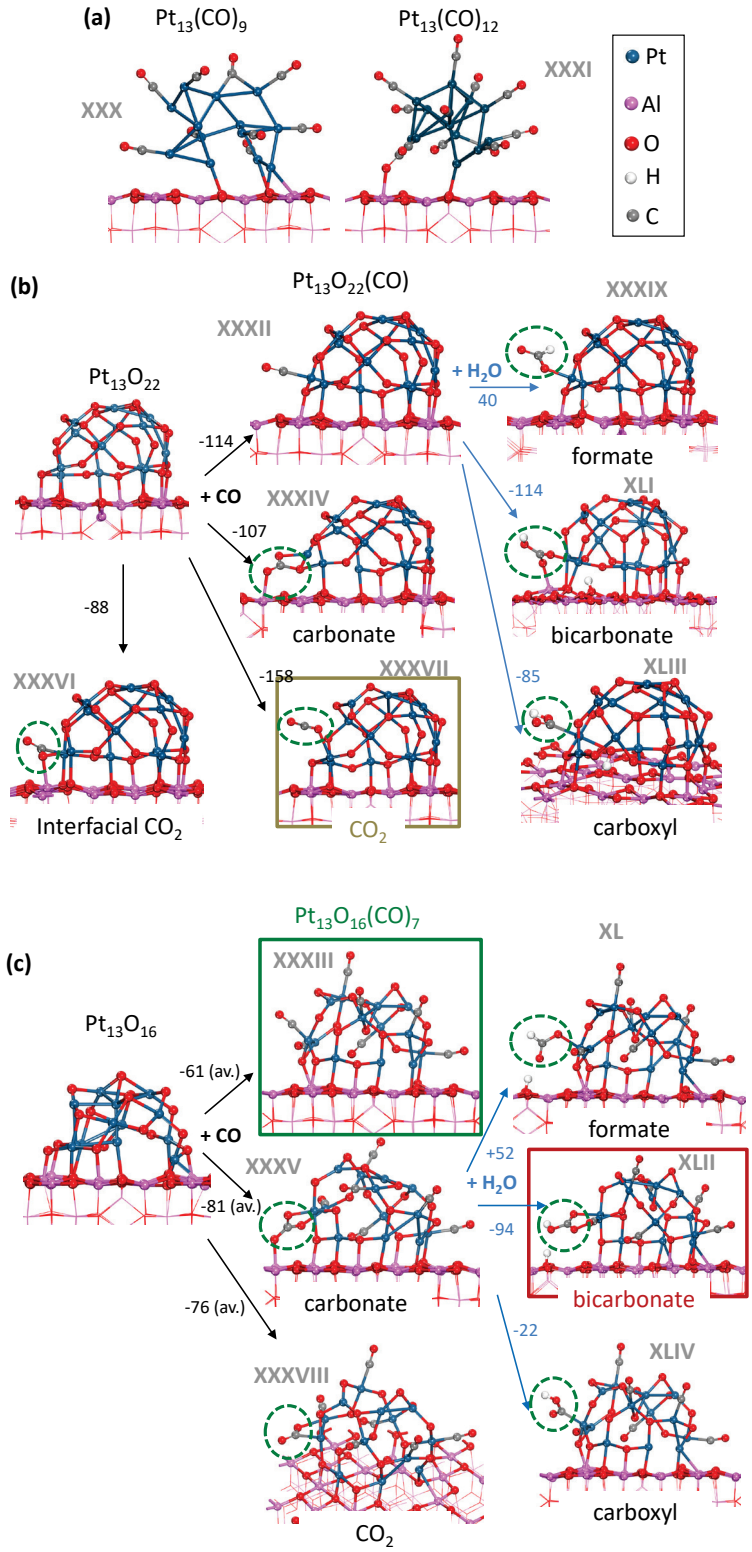

Figure 5. DFT-optimized models of CO adsorption and hydration on Pt_{13} clusters supported on alumina: a) $Pt_{13}(CO)_n$, b) $Pt_{13}O_{22}(CO)$, c) $Pt_{13}O_{16}(CO)_7$. The corresponding energy gain/loss (kJ/mol) are indicated on the arrows. The dotted green ovals locate the relevant functional group. CO adsorption energy is reported as an average value for the $Pt_{13}O_{16}(CO)_7$ case. Av. means average.

*Table 3. DFT-computed vibration wavenumbers (cm^{-1}) for selected Pt_{13} species adsorbed on alumina. Numbers in italic correspond to shifted wavenumbers (see **Section 2.4**). The intensity of the mode is reported between brackets in arbitrary units. $Pt_{13}(CO)_9$ and $Pt_{13}(CO)_{12}$ supported clusters are extracted from ref. [36]. The underlined Roman numerals correspond to the most probable species. Al atoms coordinated to ligands are not mentioned in the case of O ligand, as many Al atoms are involved in the metal/support interaction. They are mentioned only if they are present for ligands different from O.*

Carbonyl		
XXX	$Pt_{13}(CO)_9$	*2071 (13.8), 2051 (4.8), 2048 (1.1), 2043 (4.1), 2041 (3.4), 2038 (2.5), 2033 (0.2), 2032 (1.2), 1928 (8.6)*
XXXI	$Pt_{13}(CO)_{12}Al$	*2085 (26.3), 2061 (9.8), 2059 (12.6), 2047 (8.3), 2042 (3.7), 2039 (1.8), 2037 (0.5), 2033 (0.1), 2029 (0.2), 2024 (0.9), 1867 (0.9), 1700 (2.1)*
XXXII	$Pt_{13}O_{22}(CO)$	*2105 (2.7)*
XXXIII	$Pt_{13}O_{16}(CO)_7$	*2100 (3.5), 2087 (1.4), 2085 (2.0), 2074 (0.4), 2065 (1.8), 2052 (2.3), 2048 (2.0)*
Carbonate and carbonyl-carbonate		
XXXIV	$Pt_{13}O_{20}(CO_3)Al$	1699 (2.7), 1220 (0.3), 1006 (2.6), 839 (0.3)
XXXV	$Pt_{13}O_{14}(CO)_6(CO_3)Al$	*2111 (1.7), 2098 (1.8), 2080 (0.2), 2074 (4.1), 2069 (2.1), 2061 (0.1)*, 1551 (3.8), 1251 (0.1), 1056 (0.5), 990 (2.1)
Adsorbed CO_2		
XXXVI	$Pt_{13}O_{21}(CO_2)Al$	1728, 1084
XXXVII	$Pt_{13}O_{21}(CO_2)$	2344, 1294
XXXVIII	$Pt_{13}O_{15}(CO)_6(CO_2)$	*2101, 2094, 2090, 2076, 2070, 2061*, 1771, 1115
Formate and carbonyl-formate		
XXXIX	$Pt_{13}O_{22}(CO_2H)$	2758 (0.7), 1686 (0.9), 1287 (0.1), 1098 (0.1), 1039 (1.5)
XL	$Pt_{13}O_{16}(CO)_6(CO_2H)$	2940 (0.1), *2102 (3.0), 2085 (3.6), 2066 (3.0), 2062 (3.7), 2036 (1.1), 2024 (3.4)*, 1598 (2.2), 1326 (0.1), 1220 (0.9), 1010 (1.6)
Bicarbonate and carbonyl-bicarbonate		
XLI	$Pt_{13}O_{21}(CO_3H)Al$	3636 (0.3), 2813 (4.3), 1544 (0.7), 1431 (0.9), 1180 (0.9)
XLII	$Pt_{13}O_{15}(CO)_6(CO_3H)$	3649 (0.3), *2101 (3.0), 2075 (0.2), 2066 (4.9), 2055 (4.1), 2052 (0.4), 2050 (1.0)*, 1618 (0.2), 1362 (2.4), 1208 (0.9), 1022 (0.8)
Carboxyl and carbonyl-carboxyl		
XLIII	$Pt_{13}O_{22}(COOH)$	3577 (0.2), 1709 (0.4), 1271 (0.2), 1048 (2.0), 1011 (2.2)
XLIV	$Pt_{13}O_{16}(CO)_6(COOH)$	3579 (0.1), *2099 (3.2), 2081 (4.1), 2067 (1.5), 2059 (1.2), 2038 (1.4), 2012 (2.6)*, 1718 (0.7), 1273 (0.2), 1062 (2.3)

4. Discussion

We now compare the vibration frequencies and their intensities (Tables 2 and 3) with *operando* DRIFTS results, spectral zone by spectral zone, to conclude about the species in presence under the practical operating conditions.

Regarding computed vibrational wavenumbers for Pt carbonyls, the most intense contributions (computed maximal intensity 26.3 a.u.) are expected to correspond to reduced forms of Pt_{13} clusters, *i.e.* $Pt_{13}(CO)_9$ and $Pt_{13}(CO)_{12}$, in particular for the highest-frequency top sites between 2060 and 2085 cm^{-1} (Table 3). The $Pt_{13}(CO)_9$ model is consistent with the DRIFTS spectra recorded during CO desorption experiments on pre-reduced catalysts (Figure S9). After the pre-oxidation treatment applied in our case and under the subsequent CO oxidation conditions, the clusters are partially oxidized.[23] Among clusters combining oxygen and CO as co-adsorbates, the $Pt_{13}O_{16}(CO)_7$ model is the one that best represents the state of the nanocatalyst at low temperature (*i.e.* before reaction light-off from 150 °C), with respect to the more oxidized $Pt_{13}O_{22}(CO)$ model, on the basis of the comparison between experimental and computed IR features. Note, however, that the former, besides the vibrations at 2100-2085 cm^{-1}, also exhibits a significant signal close to 2050 cm^{-1} due to CO molecules that are at the interface between the cluster and the support. The lower intensity of such a signal experimentally (low-frequency shoulder) suggests that the real CO coverage is probably lower than the one simulated here. Nevertheless, the exhaustive sampling of all O/CO coverages on Pt_{13} clusters is beyond the scope of the present work.

Carbonyls held by SAs exhibit maximal intensities of the order of 1 a.u. according to our DFT calculations (Table 2), which is less intense than for clusters. $Pt_1(CO)_1$ (**II**) is expected to give rise to a signal at 2058 cm^{-1}, which splits into higher and lower frequency modes when increasing the number of adsorbed CO molecules. The computed intensities for species **III** to **V** however show that the higher-frequency modes are less intense than the low-frequency one. Thus, carbonyls held by reduced SAs should lead to detectable signals in the 2015-2075 cm^{-1} range, which is not observed experimentally (Figure 2). This holds for species **XXII**, in which CO is co-adsorbed with a formate group, and is computed at 2032 cm^{-1}. This means that either these species are not formed, or they quickly convert into

more stable species, such as clusters, as discussed previously. Oxidized forms of SAs bonded to carbonyls are at the origin of a CO elongation mode computed at a significantly higher wavenumber with respect to reduced forms, which falls in the 2084-2150 cm^{-1} interval. The highest values, close to 2150 cm^{-1}, correspond to species **XIII**, **XIV**, **XV**, **XXVII**, and **XXVIII**, in which CO co-adsorbs with carbonates or/and C_2O_4 groups, most of the time within octahedral Pt complexes (with the exception of **XIII**, which is square planar). They correspond to cases were the adsorption strength of CO (possibly including the formation of the dimer) is weak to moderate (-55 to -167 $kJ.mol^{-1}$). Their spectral feature is close to that of gas-phase CO (2143 cm^{-1}), suggesting a very weak covalent bonding between Pt and CO. Consistently, the fact that no contribution is observed experimentally close to 2150 cm^{-1} suggests that, in the present operating conditions, these species are not formed, as the computed intensities are comparable to those of other carbonyls on SACs. Other carbonyls linked to oxidized Pt (**VI**, **XII**, **XXIV**, **XXVI**, **XXIX**) give rise to signals between 2094 and 2124 cm^{-1}, which are likely to correspond to the experimental signal at 2105 cm^{-1} (Figure 2). Thus, in the end, from the analysis of the computed CO frequencies, the 2105 cm^{-1} band can be assigned to carbonyls held by oxidized clusters or/and SAs, possibly in the presence of co-adsorbates such as carbonates, carboxyls, bicarbonates, or formates.

Regarding the vibrations of carbonates, a strong overestimation of the highest computed frequency modes (ν_{CO}) with respect to experiments is systematically observed (by up to 150 cm^{-1}, see Table S1 and Figure S14), as well as an underestimation of the second mode (ν_{asCOO}), as it was reported in the literature for several kinds of carbonates with frequency estimations at the GGA level.[16,51–53] We confirmed this observation by computing the vibrational frequencies of the molecular complex reported in ref. [54] at the same level of theory as the surfaces modelled here (Table S1). Solving this problem would require going beyond the GGA level for frequency calculations. It is thus likely that the good matching between the computed frequencies at 1550 and 1250 cm^{-1} for the carbonate in $Pt_{13}O_{14}(CO)_6(CO_3)$ (species **XXXV**) and the experimentally observed ones is fortuitous, carbonates being seen for the SAC only. Notably, the simulated C_2O_4 species **XXVII** and **XXVIII** are expected to yield computed vibrational modes in the same vibrational region as carbonates, which makes these two families of species hardly

distinguishable. Assuming a maximal 150 cm^{-1} shift between experimental and computed features for the highest frequency mode makes species **IX** ($PtO_2(CO_3)$) and **XXXIV** ($Pt_{13}O_{20}(CO_3)$) relevant. Species **XII** and **XIII**, which are attractive from the thermodynamic point of view (Figure S13e) and accommodate both a carbonyl and a carbonate on the same Pt single atom, give rise to higher frequencies than species **IX** for the carbonate group, which lets the question of their experimental observation open. Similarly, species **XXIX** and **XXIV**, which are compatible with the experiments for the carbonyl signal, exhibit a higher ν_{CO} frequency for the carbonate group.

The computed wavenumbers of bicarbonates are much more comparable to the experiments. Considering non-hydrogen-bonded OH groups belonging to bicarbonates, a ν_{OH} wavenumber close to 3670 cm^{-1} for SAs (species **XVI-XX**), and between 3630 and 3650 cm^{-1} (harmonic values) for clusters (species **XLI** and **XLII**), is predicted, in very good agreement with previous estimations for bicarbonates on the Pt(111) surface.[52] The best agreement with the experimental wavenumbers at 1230, 1440 and 1655 cm^{-1} is obtained with species **XVII** ($Pt(CO_3H)$), a bidentate species bonded to Pt and Al. No general rule can be detected with respect to the ranking of the bicarbonate frequencies as a function of Pt nuclearity (SA *versus* cluster).

Carboxyls exhibit a computed harmonic O-H bond elongation frequency of 3549 cm^{-1} for the SA (species **XXIX**) and slightly lower than 3580 cm^{-1} for the clusters (**XXXVIII** and **XXXIX**). However, these bands overlap with O-H stretching ones coming from adsorbed hydroxyl groups or water molecules. In the case of species **XXIX**, as the carboxyl group is a co-ligand of Pt with a carbonate, a series of modes coupling both ligands appears between 1018 and 1771 cm^{-1}, typically in the same range as carbonates alone, thus giving rise to the same limitations in terms of comparison with experiments. Similarly, for the clusters, the carboxyl group modes fall in a similar wavenumber range as carbonates, although not coupled to other modes.

Formates (species **XXI-XXIV**) are computed to give a harmonic C-H frequency between 2968 and 3067 cm^{-1}, in agreement with experimental observations (Figure S10) and previous calculations performed on

the Ni(111) surface.[55] The greatest intensities are predicted for the COO bending modes at 1568 cm^{-1} for the Al formate and 1580 cm^{-1} for a Pt carbonyl-formate. Similar intensities are expected for these two species. Thus, the experimental observation of this band mainly on the alumina support is not due to differences in extinction coefficients but clearly demonstrates the preferred formation of formates on the support above 200 °C. In contrast, the bicarbonates initially present on Pt catalysts at low temperature are retained above 200 °C, which is consistent with their higher computed stability compared to formates (Figure 5), unlike on pure alumina (Figure 4).

Finally, species **XXV** (SA) and **XXXVII** (cluster) involve linearly adsorbed CO_2 on Pt, which exhibits an asymmetric vibration mode at 2348 and 2344 cm^{-1}, respectively, in excellent agreement with the DRIFTS signal. This weak feature is observed on all samples.

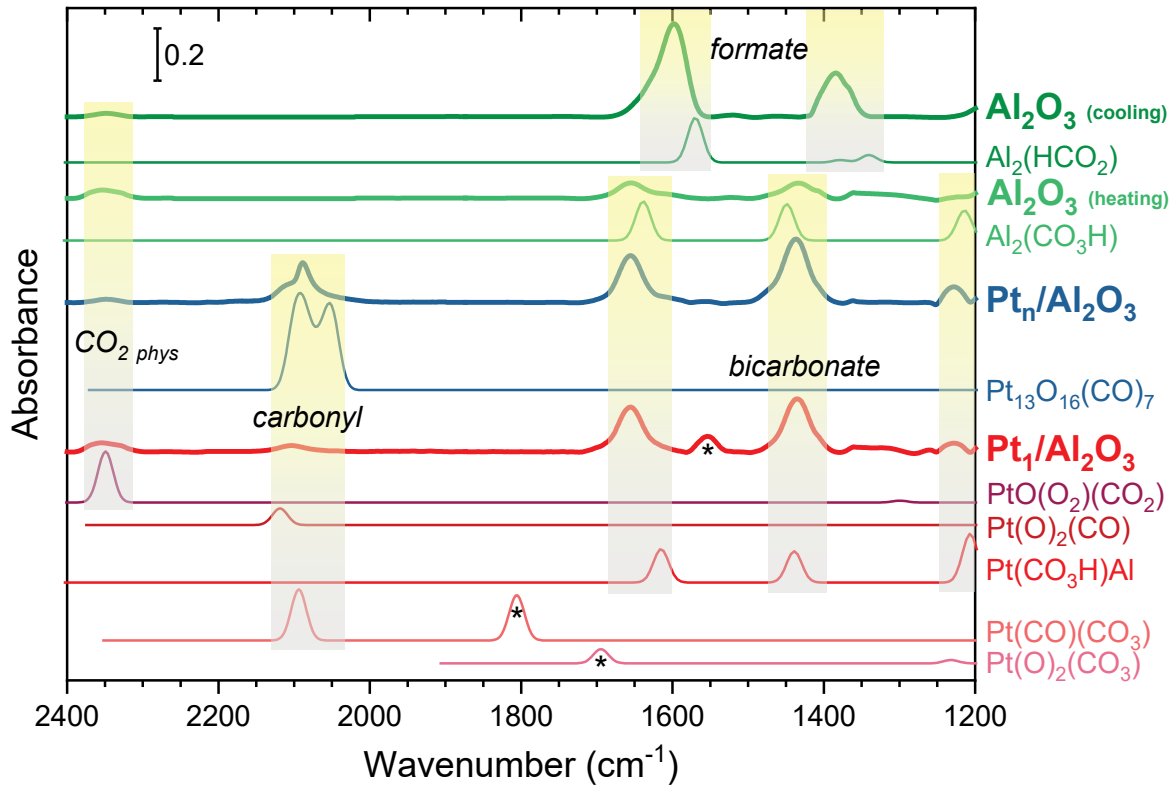

*Figure 6. Comparison between recorded DRIFTS spectra (thick lines) and computed wavenumbers (thin lines) for the most probable species. * indicates carbonate vibrations.*

The rectangles in Figures 4 and 5 identify the most probable species on the basis of the comparison of DRIFTS experiments and computed frequencies, as also summarized in Figure 6 showing representative spectra and computed band positions. The latter comparison shows the good agreement between experiment and theory regarding bicarbonate (CO_3H) and formate (CO_2H) species, the latter being mostly formed on alumina (species **XXI**). As for CO chemisorption and CO_3 formation on Pt SAs, the comparison of thermodynamic features (Figure S13e) is favorable to co-adsorption (species **XII** and **XIII**) *versus* separate adsorption. The energy gains for CO adsorption are also much stronger on SAs than on clusters, according to DFT. The similarity in experimental thermal behaviors of Pt-CO and Pt-CO_3 bands for the SAC (Figure 3) additionally suggests that Pt SAs simultaneously accommodate both chemical groups in the form of a Pt carbonyl-carbonate species resembling the one represented in Figure 4 (species **XII** and **XIII**), even if the computed frequencies are more in agreement (though with large differences for the carbonates) with species independently adsorbed on the SAC (species **VI** and **IX**). Notably, the need for a positive initial Pt oxidation state for co-adsorbing CO_3 and CO groups (Figure 4) can explain the negligible fraction of carbonyl species present on the SAC with respect to carbonates in CO desorption experiments, *i.e.* in the absence of O_2 (Figures S8 and S9).

As far as the intrinsic activity of the SAs is concerned, consistently with our previous one,[23] this work suggests that they are inactive spectator species. Newton *et al.* reported a release of CO_2 under CO at RT, and ascribe it to the $Pt(CO_3) \rightarrow Pt(O) + CO_2$ reaction.[18] In their transient process, the single Pt atom is thought to be regenerated under O_2 to $Pt(O)_2$ thanks to the neighboring presence of Pt NPs which enable O_2 dissociation as well as CO storage; $Pt(O)_2$ is then converted back to $Pt(CO_3)$ under the next CO pulse. Nonetheless, while – as in our case – bidentate carbonate formation from CO adsorption on $Pt(O_2)$ was found exo-energetic by Moses deBusk *et al.*, CO_2 formation from $Pt(CO_3)$ is endo-energetic (2.22 eV).[16] According to our calculations, a similar transient CO_2 release may occur from the interaction of Pt_1O_4 with CO through species **XXV** (Figure 4), *i.e.* without involving a Pt carbonate. A weak CO_2 signal was detected at 20-50 °C in our experiments, but it is present both on the SAC and the NC and even on pure alumina (Figure 2), and it is rather ascribed to physisorbed CO_2 (Figure 6).

Also from DFT, Gao proposed the formation of a bidentate Pt(O*–O–C*=O) species,[56] similar to the ones suggested by Allian *et al.* [57] and Yin *et al.*[58] for Pt clusters. We computed such a species from Pt_1O_2, corresponding to a CO adsorption energy of -141 kJ.mol^{-1} (not shown). It is thus a high-energy intermediate with respect to species **VI** and **VIII**. CO_2 could be evolved from this instable species, which however was not experimentally detected. Instead, the carbonate species detected on the SAC by DRIFTS is present at all temperatures and not correlated to CO_2 formation. Finally, bicarbonate species may contribute to CO_2 evolution at high temperature, but they are not specific to the SAC.

Both experimental and theoretical results indicate that Pt single atoms are poisoned by carbonyl and carbonate species. On the DRIFTS side, Figure 2 and Figure 3 show that these species are present throughout the temperature cycle on SAs, whereas their coverage is very low (Pt-CO) or zero (Pt-CO_3) on the NPs during the reaction. From DFT calculations, Figure 4 and Figure 5 report that carbonyl and carbonate adsorption energies are much higher on the SAs than on the NPs. Hence, these results rationalize the poor activity found for the SAs compared to the NPs.[17,23]

5. Conclusions

We have reported a thorough experimental (DRIFTS) and theoretical (DFT) study aiming at understanding the nature and evolution of adsorbed carbon-containing molecular species, beyond the simple Pt-CO carbonyl, at the surface of the prototypical Pt/Al_2O_3 SAC system under CO oxidation conditions, in comparison to a nanocatalyst counterpart. Whereas the nanocatalyst is covered by active Pt-CO carbonyl and mostly spectator HCO_3 bicarbonate species (1655, 1440 and 1230 cm^{-1}), the SAC additionally exhibits a high concentration of carbonate species. Moreover, the Pt_1-CO (2105 cm^{-1}) and Pt_1-CO_3 (1550 and 1250 cm^{-1}) IR features are highly correlated and both of them are essentially spectators.

DFT calculations indicate that the most probable carbonyl and bicarbonate species in the SAC are Pt_1O_2-CO (2119 cm^{-1}) and Pt_1-(CO_3H)-Al (1610, 1435 and 1188 cm^{-1}), respectively. For carbonates, the

comparison with experiments is made difficult by the known inability of DFT to predict carbonate vibration modes, that we substantiate in this work. From a spectroscopic viewpoint, the least unfavorable candidate with respect to the experimental results is a Pt_1O_2-CO_3 chelating bidentate carbonate (1691 and 1228 cm^{-1}), which would coexist with the Pt_1O_2-CO species. However, from thermodynamic (adsorption energies) and experimental (simultaneous thermal evolution of IR intensities) arguments, the calculations point to hybrid carbonate-carbonyl species, OC-Pt_1-CO_3-Al and $(OC)_2$-Pt_1-CO_3-Al. These adsorbates are derived from an already stable Pt-CO_3 chelating bidentate Pt carbonate (energy gain of 466 kJ/mol with respect to Pt_1O_2), but with additional energy gain(s) of 137 kJ/mol (137+102 kJ/mol) upon addition of one (two) CO molecule(s).

Reduced forms of Pt SA were computed to be thermodynamically unstable under CO atmosphere, with a tendency to clustering, consistently with experiments. Supported Pt_{13}, $Pt_{13}O_{16}$ and $Pt_{13}O_{22}$ cluster models were used to understand the behavior of nanocatalysts. The $Pt_{13}O_{16}$ stoichiometry leads to computed frequencies for adsorbed carbonyls, $Pt_{13}O_{16}(CO)_7$, that show the best agreement with experiments in CO oxidation atmosphere for temperatures below 150 °C. Bicarbonates are also likely formed on (or at the periphery of) such clusters in the same conditions.

Whether co-adsorbed on the same Pt atom or independently adsorbed, the high stability of carbonyl and carbonates moieties on single atoms, much higher than on clusters, can explain the much lower activity of Pt/alumina SACs for CO oxidation in comparison with nanocatalysts.

Author information

Corresponding authors:

- Laurent Piccolo, IRCELYON, CNRS & Université Lyon 1, 69100 Villeurbanne, France; orcid.org/0000-0003-4095-0572; Email: laurent.piccolo@ircelyon.univ-lyon1.fr

- Céline Chizallet, IFP Energies nouvelles, Rond-point de l'échangeur de Solaize, 69360 Solaize, France; orcid.org/0000-0001-5140-8397; Email: celine.chizallet@ifpen.fr

Other authors:

- Franck Morfin, IRCELYON, CNRS & Université Lyon 1, 69100 Villeurbanne, France; orcid.org/0000-0003-3272-708X
- Caroline Dessal, IRCELYON, CNRS & Université Lyon 1, 69100 Villeurbanne, France
- Alexis Sangnier, IFP Energies nouvelles, Rond-point de l'échangeur de Solaize, 69360 Solaize, France

Associated content

Supporting information: Protocol of CO oxidation experiments on Pt/Al_2O_3 catalysts, detailed DRIFTS data, identification of formate species, distribution of the computed frequencies, computed thermodynamic diagrams, experimental *versus* computed frequencies for species containing carbonates as reported in the literature.

Acknowledgements

Agence Nationale de la Recherche (UltraCat project, ANR-17-CE06-0008) is acknowledged for financial support of the experiments. M. Aouine and CLYM are acknowledged for STEM analyses. R. Checa is acknowledged for technical support. Calculations were performed using HPC resources from GENCI-CINES (Grant A0120806134) and from IFP Energies nouvelles (ENER440). AS and CC thank C. Dujardin (UCCS Lille) and M. Matrat (IFPEN) for fruitful discussions.

References

(1) Liu, J. Catalysis by Supported Single Metal Atoms. *ACS Catal.* **2017**, *7*, 34–59. https://doi.org/10.1021/acscatal.6b01534.

(2) Wang, A.; Li, J.; Zhang, T. Heterogeneous Single-Atom Catalysis. *Nat. Rev. Chem.* **2018**, *2* (6), 65–81. https://doi.org/10.1038/s41570-018-0010-1.

(3) Kaiser, S. K.; Chen, Z.; Faust Akl, D.; Mitchell, S.; Pérez-Ramírez, J. Single-Atom Catalysts across the Periodic Table. *Chem. Rev.* **2020**, *120* (21), 11703–11809. https://doi.org/10.1021/acs.chemrev.0c00576.

(4) Zhang, H.; Fang, S.; Hu, Y. H. Recent Advances in Single-Atom Catalysts for CO Oxidation. *Catal. Rev. Sci. Eng.* **2020**, *64* (3), 491–532. https://doi.org/10.1080/01614940.2020.1821443.

(5) *Supported Metal Single Atom Catalysis, First Edition*, P. Serp&D. Pham Minh (Eds.).; Wiley-VCH: Weinheim, 2021.

(6) Di Liberto, G.; Pacchioni, G. Modeling Single-Atom Catalysis. *Adv. Mater.* **2023**, *35* (46), 2307150. https://doi.org/10.1002/adma.202307150.

(7) Wovchko, E. A.; Yates, J. T. Activation of O2 on a Photochemically Generated RhI Site on an Al2O3 Surface: Low-Temperature O2 Dissociation and CO Oxidation. *J. Am. Chem. Soc.* **1998**, *120* (40), 10523–10527. https://doi.org/10.1021/ja981241y.

(8) Asakura, K.; Nagahiro, H.; Ichikuni, N.; Iwasawa, Y. Structure and Catalytic Combustion Activity of Atomically Dispersed Pt Species at MgO Surface. *Appl. Catal. A* **1999**, *188* (1), 313–324. https://doi.org/10.1016/S0926-860X(99)00247-1.

(9) Abbet, S.; Heiz, U.; Häkkinen, H.; Landman, U. CO Oxidation on a Single Pd Atom Supported on Magnesia. *Phys. Rev. Lett.* **2001**, *86* (26), 5950–5953. https://doi.org/10.1103/PhysRevLett.86.5950.

(10) Fu, Q.; Saltsburg, H.; Flytzani-Stephanopoulos, M. Active Nonmetallic Au and Pt Species on Ceria-Based Water-Gas Shift Catalysts. *Science* **2003**, *301* (5635), 935–938. https://doi.org/10.1126/science.1085721.

(11) Hackett, S. F. J.; Brydson, R. M.; Gass, M. H.; Harvey, I.; Newman, A. D.; Wilson, K.; Lee, A. F. High-Activity, Single-Site Mesoporous Pd/Al2O3 Catalysts for Selective Aerobic Oxidation of Allylic Alcohols. *Angew. Chem. Int. Ed.* **2007**, *46* (45), 8593–8596. https://doi.org/10.1002/anie.200702534.

(12) Aguilar-Guerrero, V.; Gates, B. C. Kinetics of CO Oxidation Catalyzed by Highly Dispersed CeO2-Supported Gold. *J. Catal.* **2008**, *260* (2), 351–357. https://doi.org/10.1016/j.jcat.2008.09.012.

(13) Tang, W.; Hu, Z.; Wang, M.; Stucky, G. D.; Metiu, H.; McFarland, E. W. Methane Complete and Partial Oxidation Catalyzed by Pt-Doped CeO2. *J. Catal.* **2010**, *273* (2), 125–137. https://doi.org/10.1016/j.jcat.2010.05.005.

(14) Qiao, B.; Wang, A.; Yang, X.; Allard, L. F.; Jiang, Z.; Cui, Y.; Liu, J.; Li, J.; Zhang, T. Single-Atom Catalysis of CO Oxidation Using Pt_1/FeO_x. *Nat. Chem.* **2011**, *3* (8), 634–641. https://doi.org/10.1038/nchem.1095.

(15) Piccolo, L.; Loridant, S.; Christopher, P. Supported Metal Single-Atom Thermocatalysts for Oxidation Reactions. In *Supported Metal Single Atom Catalysis*; John Wiley & Sons, Ltd, 2022; pp 377–423. https://doi.org/10.1002/9783527830169.ch9.

(16) Moses-DeBusk, M.; Yoon, M.; Allard, L. F.; Mullins, D. R.; Wu, Z.; Yang, X.; Veith, G.; Stocks, G. M.; Narula, C. K. CO Oxidation on Supported Single Pt Atoms: Experimental and Ab Initio Density Functional Studies of CO Interaction with Pt Atom on θ-Al_2O_3(010) Surface. *J. Am. Chem. Soc.* **2013**, *135* (34), 12634–12645. https://doi.org/10.1021/ja401847c.

(17) Ding, K.; Gulec, A.; Johnson, A. M.; Schweitzer, N. M.; Stucky, G. D.; Marks, L. D.; Stair, P. C. Identification of Active Sites in CO Oxidation and Water-Gas Shift over Supported Pt Catalysts. *Science* **2015**, *350* (6257), 189–192. https://doi.org/10.1126/science.aac6368.

(18) Newton, M. A.; Ferri, D.; Smolentsev, G.; Marchionni, V.; Nachtegaal, M. Room-Temperature Carbon Monoxide Oxidation by Oxygen over Pt/Al_2O_3 Mediated by Reactive Platinum Carbonates. *Nat. Commun.* **2015**, *6*, 8675. https://doi.org/10.1038/ncomms9675.

(19) Newton, M. A.; Ferri, D.; Smolentsev, G.; Marchionni, V.; Nachtegaal, M. Kinetic Studies of the Pt Carbonate-Mediated, Room-Temperature Oxidation of Carbon Monoxide by Oxygen over Pt/Al_2O_3 Using Combined, Time-Resolved XAFS, DRIFTS, and Mass Spectrometry. *J. Am. Chem. Soc.* **2016**, *138* (42), 13930–13940. https://doi.org/10.1021/jacs.6b06819.

(20) Lou, Y.; Liu, J. CO Oxidation on Metal Oxide Supported Single Pt Atoms: The Role of the Support. *Ind. Eng. Chem. Res.* **2017**, *56* (24), 6916–6925. https://doi.org/10.1021/acs.iecr.7b01477.

(21) Zhang, Z.; Zhu, Y.; Asakura, H.; Zhang, B.; Zhang, J.; Zhou, M.; Han, Y.; Tanaka, T.; Wang, A.; Zhang, T.; Yan, N. Thermally Stable Single Atom $Pt/m\text{-}Al_2O_3$ for Selective Hydrogenation and CO Oxidation. *Nat. Commun.* **2017**, *8*, 16100. https://doi.org/10.1038/ncomms16100.

(22) Wang, H.; Dong, J.; Allard, L. F.; Lee, S.; Oh, S.; Wang, J.; Li, W.; Shen, M.; Yang, M. Single-Site Pt/La-Al2O3 Stabilized by Barium as an Active and Stable Catalyst in Purifying CO and C3H6 Emissions. *Appl. Catal. B* **2019**, *244*, 327–339. https://doi.org/10.1016/j.apcatb.2018.11.034.

(23) Dessal, C.; Len, T.; Morfin, F.; Rousset, J.-L.; Aouine, M.; Afanasiev, P.; Piccolo, L. Dynamics of Single Pt Atoms on Alumina during CO Oxidation Monitored by Operando X-Ray and Infrared Spectroscopies. *ACS Catal.* **2019**, *9*, 5752–5759. https://doi.org/10.1021/acscatal.9b00903.

(24) Kresse, G.; Hafner, J. Ab Initio Molecular-Dynamics Simulation of the Liquid-Metal–Amorphous-Semiconductor Transition in Germanium. *Phys. Rev. B* **1994**, *49* (20), 14251–14269. https://doi.org/10.1103/PhysRevB.49.14251.

(25) Kresse, G.; Furthmüller, J. Efficiency of Ab-Initio Total Energy Calculations for Metals and Semiconductors Using a Plane-Wave Basis Set. *Comput. Mater. Sci.* **1996**, *6* (1), 15–50. https://doi.org/10.1016/0927-0256(96)00008-0.

(26) Perdew, J. P.; Burke, K.; Ernzerhof, M. Generalized Gradient Approximation Made Simple. *Phys. Rev. Lett.* **1996**, *77* (18), 3865–3868. https://doi.org/10.1103/PhysRevLett.77.3865.

(27) Kresse, G.; Joubert, D. From Ultrasoft Pseudopotentials to the Projector Augmented-Wave Method. *Phys. Rev. B* **1999**, *59* (3), 1758–1775. https://doi.org/10.1103/PhysRevB.59.1758.

(28) Digne, M.; Sautet, P.; Raybaud, P.; Euzen, P.; Toulhoat, H. Hydroxyl Groups on γ-Alumina Surfaces: A DFT Study. *J .Catal.* **2002**, *211* (1), 1–5. https://doi.org/10.1006/jcat.2002.3741.

(29) Digne, M.; Sautet, P.; Raybaud, P.; Euzen, P.; Toulhoat, H. Use of DFT to Achieve a Rational Understanding of Acid-Basic Properties of γ-Alumina Surfaces. *J. Catal.* **2004**, *226* (1), 54–68. https://doi.org/10.1016/j.jcat.2004.04.020.

(30) Mager-Maury, C.; Chizallet, C.; Sautet, P.; Raybaud, P. Platinum Nanoclusters Stabilized on γ-Alumina by Chlorine Used as a Capping Surface Ligand: A Density Functional Theory Study. *ACS Catal.* **2012**, *2* (7), 1346–1357. https://doi.org/10.1021/cs300178y.

(31) Hu, C. H.; Chizallet, C.; Mager-Maury, C.; Corral-Valero, M.; Sautet, P.; Toulhoat, H.; Raybaud, P. Modulation of Catalyst Particle Structure upon Support Hydroxylation: Ab Initio Insights into Pd_{13} and $Pt_{13}/\gamma\text{-}Al_2O_3$. *J. Catal.* **2010**, *274* (1), 99–110. https://doi.org/10.1016/j.jcat.2010.06.009.

(32) Lagauche, M.; Larmier, K.; Jolimaitre, E.; Barthelet, K.; Chizallet, C.; Favergeon, L.; Pijolat, M. Thermodynamic Characterization of the Hydroxyl Group on the γ-Alumina Surface by the Energy Distribution Function. *The Journal of Physical Chemistry C* **2017**, *121* (31), 16770–16782. https://doi.org/10.1021/acs.jpcc.7b02498.

(33) Pigeon, T.; Chizallet, C.; Raybaud, P. Revisiting γ-Alumina Surface Models through the Topotactic Transformation of Boehmite Surfaces. *Journal of Catalysis* **2022**, *405*, 140–151. https://doi.org/10.1016/j.jcat.2021.11.011.

(34) Mager-Maury, C.; Bonnard, G.; Chizallet, C.; Sautet, P.; Raybaud, P. H_2-Induced Reconstruction of Supported Pt Clusters: Metal–Support Interaction versus Surface Hydride. *ChemCatChem* **2011**, *3* (1), 200–207. https://doi.org/10.1002/cctc.201000324.

(35) Sangnier, A.; Matrat, M.; Nicolle, A.; Dujardin, C.; Chizallet, C. Multiscale Approach to the Dissociative Adsorption of Oxygen on Highly Dispersed Platinum Supported on γ-Al2O3. *J. Phys. Chem. C* **2018**, *122*, 26974–26968. https://doi.org/10.1021/acs.jpcc.8b09204.

(36) Sangnier, A.; Genty, E.; Iachella, M.; Sautet, P.; Raybaud, P.; Matrat, M.; Dujardin, C.; Chizallet, C. Thermokinetic and Spectroscopic Mapping of Carbon Monoxide Adsorption on Highly Dispersed Pt/γ-Al2O3. *ACS Catal.* **2021**, 13280–13293. https://doi.org/10.1021/acscatal.1c04262.

(37) Gorczyca, A.; Moizan, V.; Chizallet, C.; Proux, O.; Del Net, W.; Lahera, E.; Hazemann, J.-L.; Raybaud, P.; Joly, Y. Monitoring Morphology and Hydrogen Coverage of Nanometric Pt/γ-Al_2O_3 Particles by in Situ HERFD–XANES and Quantum Simulations. *Angew. Chem. Int. Ed.* **2014**, *53* (46), 12426–12429. https://doi.org/10.1002/anie.201403585.

(38) Dessal, C.; Sangnier, A.; Chizallet, C.; Dujardin, C.; Morfin, F.; Rousset, J.-L.; Aouine, M.; Bugnet, M.; Afanasiev, P.; Piccolo, L. Atmosphere-Dependent Stability and Mobility of Catalytic Pt Single Atoms and Clusters on γ-Al_2O_3. *Nanoscale* **2019**, *11* (14), 6897–6904. https://doi.org/10.1039/C9NR01641D.

(39) Hellier, A.; Batista, A. T. F.; Legens, C.; Tapia, A. A.; Proux, O.; Hazemann, J.-L.; Gay, A.-S.; Joly, Y.; Chizallet, C.; Raybaud, P. Identification of Oxidized Platinum Single Atoms on Chlorinated γ–Alumina Support by Density Functional Theory Calculations and X-Ray Absorption Spectroscopy. *J. Catal.* **2024**, *429*, 115212. https://doi.org/10.1016/j.jcat.2023.115212.

(40) Föttinger, K.; Emhofer, W.; Lennon, D.; Rupprechter, G. Adsorption and Reaction of CO on (Pd–)Al2O3 and (Pd–)ZrO2: Vibrational Spectroscopy of Carbonate Formation. *Top. Catal.* **2017**, *60* (19), 1722–1734. https://doi.org/10.1007/s11244-017-0852-7.

(41) Iordan, A.; Zaki, M. I.; Kappenstein, C. Formation of Carboxy Species at CO/Al2O3 Interfaces. Impacts of Surface Hydroxylation, Potassium Alkalization and Hydrogenation as Assessed by in Situ FTIR Spectroscopy. *Phys. Chem. Chem. Phys.* **2004**, *6* (9), 2502–2512. https://doi.org/10.1039/B401367K.

(42) Hadjiivanov, K. I.; Vayssilov, G. N. Characterization of Oxide Surfaces and Zeolites by Carbon Monoxide as an IR Probe Molecule. In *Advances in Catalysis*; Academic Press, 2002; Vol. 47, pp 307–511. https://doi.org/10.1016/S0360-0564(02)47008-3.

(43) Groppo, E.; Rojas-Buzo, S.; Bordiga, S. The Role of In Situ/Operando IR Spectroscopy in Unraveling Adsorbate-Induced Structural Changes in Heterogeneous Catalysis. *Chem. Rev.* **2023**, *123* (21), 12135–12169. https://doi.org/10.1021/acs.chemrev.3c00372.

(44) Knözinger, H.; Ratnasamy, P. Catalytic Aluminas: Surface Models and Characterization of Surface Sites. *Catalysis Reviews* **1978**, *17* (1), 31–70. https://doi.org/10.1080/03602457808080878.

(45) Busca, G.; Lorenzelli, V.; Escribano, V. S.; Guidetti, R. FT-113 Study of the Surface Properties of the Spinels NiAl2O4 and CoAl2O4 in Relation to Those of Transitional Aluminas. *J. Catal.* **1991**, *131* (1), 167–177. https://doi.org/10.1016/0021-9517(91)90333-Y.

(46) Busca, G. The Surface of Transitional Aluminas: A Critical Review. *Catal. Today* **2014**, *226*, 2–13. https://doi.org/10.1016/j.cattod.2013.08.003.

(47) Hadjiivanov, K. Chapter Two - Identification and Characterization of Surface Hydroxyl Groups by Infrared Spectroscopy. In *Advances in Catalysis*; Jentoft, F. C., Ed.; Academic Press, 2014; Vol. 57, pp 99–318. https://doi.org/10.1016/B978-0-12-800127-1.00002-3.

(48) Thang, H. V.; Pacchioni, G.; DeRita, L.; Christopher, P. Nature of Stable Single Atom Pt Catalysts Dispersed on Anatase TiO_2. *J. Catal.* **2018**, *367*, 104–114. https://doi.org/10.1016/j.jcat.2018.08.025.

(49) Batista, A. T. F.; Wisser, D.; Pigeon, T.; Gajan, D.; Diehl, F.; Rivallan, M.; Catita, L.; Gay, A.-S.; Lesage, A.; Chizallet, C.; Raybaud, P. Beyond γ-Al2O3 Crystallite Surfaces: The Hidden Features of Edges Revealed by Solid-State 1H NMR and DFT Calculations. *J. Catal.* **2019**, *378*, 140–143. https://doi.org/10.1016/j.jcat.2019.08.009.

(50) Batista, A. T. F.; Pigeon, T.; Meyet, J.; Wisser, D.; Rivallan, M.; Gajan, D.; Catita, L.; Diehl, F.; Gay, A.-S.; Chizallet, C.; Lesage, A.; Raybaud, P. Structure, Location, and Spatial Proximities

of Hydroxyls on γ-Alumina Crystallites by High-Resolution Solid-State NMR and DFT Modeling: Why Edges Hold the Key. *ACS Catal.* **2023**, *13* (10), 6536–6548. https://doi.org/10.1021/acscatal.3c00495.

(51) Markovits, A.; García-Hernández, M.; Ricart, J. M.; Illas, F. Theoretical Study of Bonding of Carbon Trioxide and Carbonate on Pt(111): Relevance to the Interpretation of "in Situ" Vibrational Spectroscopy. *J. Phys. Chem. B* **1999**, *103* (3), 509–518. https://doi.org/10.1021/jp984016b.

(52) Berná, A.; Rodes, A.; Feliu, J. M.; Illas, F.; Gil, A.; Clotet, A.; Ricart, J. M. Structural and Spectroelectrochemical Study of Carbonate and Bicarbonate Adsorbed on Pt(111) and Pd/Pt(111) Electrodes. *J. Phys. Chem. B* **2004**, *108* (46), 17928–17939. https://doi.org/10.1021/jp048082r.

(53) Korhonen, S. T.; Calatayud, M.; Krause, A. O. I. Structure and Stability of Formates and Carbonates on Monoclinic Zirconia: A Combined Study by Density Functional Theory and Infrared Spectroscopy. *J. Phys. Chem. C* **2008**, *112* (41), 16096–16102. https://doi.org/10.1021/jp803353v.

(54) Andrews, M. A.; Gould, G. L.; Klooster, W. T.; Koenig, K. S.; Voss, E. J. Syntheses, Spectra, and Structures of (Diphosphine)Platinum(II) Carbonate Complexes. *Inorg. Chem.* **1996**, *35* (19), 5478–5483. https://doi.org/10.1021/ic9603159.

(55) Luo, Q.; Feng, G.; Beller, M.; Jiao, H. Formic Acid Dehydrogenation on Ni(111) and Comparison with Pd(111) and Pt(111). *J. Phys. Chem. C* **2012**, *116* (6), 4149–4156. https://doi.org/10.1021/jp209998r.

(56) Gao, H. CO Oxidation Mechanism on the γ-Al2O3 Supported Single Pt Atom: First Principle Study. *Appl. Surf. Sci.* **2016**, *379*, 347–357. https://doi.org/10.1016/j.apsusc.2016.04.009.

(57) Allian, A. D.; Takanabe, K.; Fujdala, K. L.; Hao, X.; Truex, T. J.; Cai, J.; Buda, C.; Neurock, M.; Iglesia, E. Chemisorption of CO and Mechanism of CO Oxidation on Supported Platinum Nanoclusters. *J. Am. Chem. Soc.* **2011**, *133* (12), 4498–4517. https://doi.org/10.1021/ja110073u.

(58) Yin, C.; Negreiros, F. R.; Barcaro, G.; Beniya, A.; Sementa, L.; Tyo, E. C.; Bartling, S.; Meiwes-Broer, K.-H.; Seifert, S.; Hirata, H.; Isomura, N.; Nigam, S.; Majumder, C.; Watanabe, Y.; Fortunelli, A.; Vajda, S. Alumina-Supported Sub-Nanometer Pt10 Clusters: Amorphization and Role of the Support Material in a Highly Active CO Oxidation Catalyst. *J. Mater. Chem. A* **2017**, *5* (10), 4923–4931. https://doi.org/10.1039/C6TA10989F.

TOC graphic

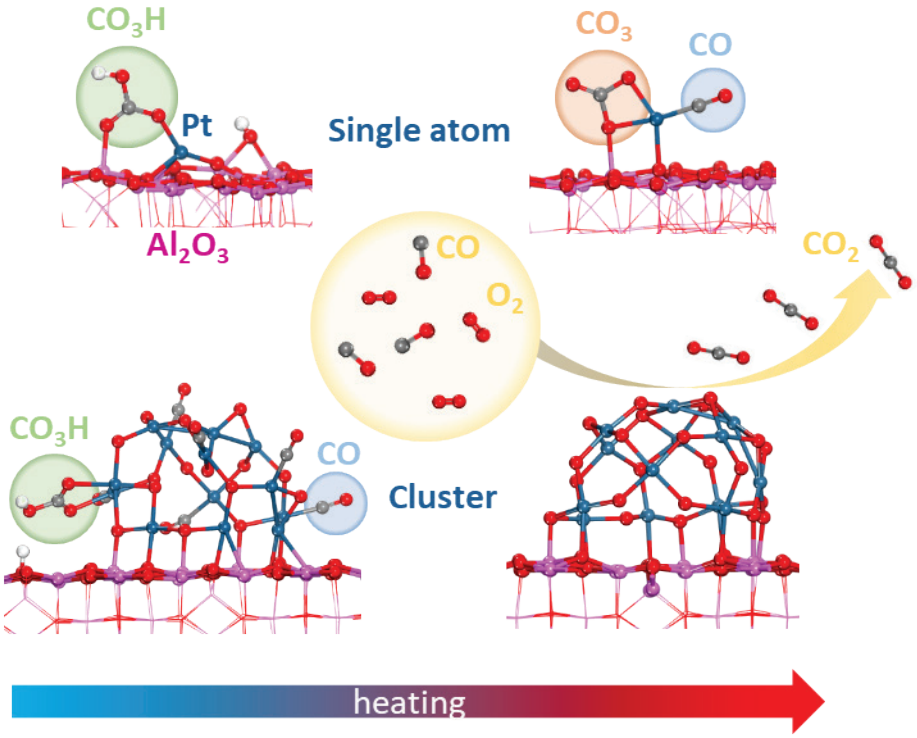
CO_3H
Pt
Al_2O_3
Single atom
CO_3
CO
CO
O_2
CO_2
CO_3H
CO
Cluster
heating